Structure and Energetics of $LiBH_4$ and Its Surfaces: A First-Principles Study†

Qingfeng Ge*

Department of Chemistry and Biochemistry, Southern Illinois University, Carbondale, Illinois 62901

Received: March 16, 2004; In Final Form: May 3, 2004

The structure and energetics of $LiBH_4$ and its surfaces have been studied using the density functional theory (DFT) plane-wave method. The DFT relaxed bulk $LiBH_4$ structure is in agreement with the synchrotron X-ray diffraction results. Four low-index surfaces, (100), (010), (001), and (101), have been created from the relaxed bulk structure. The (010), (100), and (101) surfaces were found to have a similar surface energy, $\sim$0.12 J/m^2, and are significantly more stable than the (001) surface. The H vacancy formation energies on the low-energy surfaces have been found in a narrow range of 180−200 kJ/mol. The formation energy for the first H vacancy on the (001) surface is 165.8 kJ/mol and is the lowest among all the surfaces.

1. Introduction

One of the most significant barriers to the widespread application of hydrogen fuel cell powered vehicles is the lack of practical on-board hydrogen storage systems that can provide the needed quantity of hydrogen with acceptable volume, weight, cost, and safety risk as compared with the current petrol-driven combustion engine. Appropriate thermodynamics, fast kinetics, and high storage capacities and densities are among the requirements for an effective on-board hydrogen storage system.[1] Each of the current available hydrogen storage modalities, including compressed gaseous hydrogen, cryogenic liquid hydrogen, metal hydrides, and complex hydrides, meets some of the requirements, but none meet all of them.[1−3] Both "physical" (nondissociative) and "chemical" (dissociative) storage approaches fail to offer clear advantages over hydrogen compression and liquefaction. Therefore, developing a compact and efficient hydrogen storage technology is key for hydrogen-based propulsion.

Solid-state hydrogen storage offers perhaps the best opportunities for meeting the requirements of on-board application. Over the past forty years, the focus of solid-state hydrogen storage materials has been almost exclusively on metals and metallic alloys,[4−26] in which the metal matrix provides a framework for absorbed hydrogen atoms. Most metal matrixes investigated to date, however, consist of relatively heavy elements, and gravimetric hydrogen storage capacities usually do not exceed 2 wt % when transition metals are the primary components. The alkali metal alanates and borohydrides are compounds belonging to a larger class of complex hydrides. In the past, they were known to liberate copious amounts of hydrogen either by direct thermal decomposition or hydrolysis.[27] However, these processes were generally considered irreversible and, therefore, not useful for practical hydrogen storage applications.

This bleak outlook was persisted until Bogdanovic et al. demonstrated that $NaAlH_4$ would reversibly desorb and absorb hydrogen under relatively mild conditions when it is doped with Ti-based catalysts.[28] Unlike the interstitial intermetallic hydrides, the alanates release hydrogen through a series of decomposition/recombination reactions

$$NaAlH_4 \rightleftarrows {}^1/_3Na_3AlH_6 + {}^2/_3Al + H_2 \qquad (3.7\ \text{wt\%}) \quad \text{(R1)}$$

$${}^1/_3Na_3AlH_6 \rightleftarrows NaH + {}^1/_3Al + {}^1/_2H_2 \qquad (1.9\ \text{wt\%}) \quad \text{(R2)}$$

$$NaH \rightleftarrows Na + {}^1/_2H_2 \qquad (1.9\ \text{wt\%}) \quad \text{(R3)}$$

The first two combined reactions give a theoretical hydrogen storage capacity of 5.6 wt % at low to medium temperatures (<250 °C) out of a total content of 7.5 wt %. The third step, the decomposition of NaH, occurs at temperatures above 400 °C, which is considered too high for most technical applications.[29] The reaction mechanism is based on the reversible decomposition processes in which all of the elements are mobile during reactions. This mechanism is significantly different from the hydrogen storage mechanism in the conventional metal hydrides in which hydrogen atoms are the only mobile species.

Since the breakthrough of Bogdanovic and co-workers, there has been a growing body of work in characterizing catalyzed alanates as well as developing new catalysts and new methods of preparation.[29−47] Experimental studies have been attempted to evaluate the effect of Ti-based dopants on the structure and hydrogen storage characteristics. The results showed that the rates of hydrogen absorption and desorption are strongly dependent on the level of catalyst doping,[46−48] while the total reversible hydrogen capacity decreases as the Ti−halide doping level is increased.[46] Many types of dopants result in enhanced hydrogen release/uptake kinetics to alanates. However, the mechanism of this enhancement is not clear. X-ray diffraction results seem to indicate that Ti is a substitute in the lattice of Ti-doped $NaAlH_4$.[49] Attempts have also been made to identify the active species among Ti^0, Ti^{3+}, and Ti,$^{4+}$, but to date such attempts have not been successful.[38] Clearly, a more fundamental understanding of the mechanisms that govern catalytic hydrogen adsorption/desorption in these materials is needed to help develop more rational strategies for designing novel hydrogen storage materials with dramatically improved performance.

In an effort to widen the search for more hydrogen storage candidates, other alanates and $LiBH_4$ have been explored.[50−54] $LiBH_4$ has an intrinsic hydrogen capacity of 18 wt %, which is

† Part of the "Gert D. Billing Memorial Issue".

* To whom correspondence may be addressed. Email: qge@chem.siu.edu. Fax: 618-453-6408.

10.1021/jp048829d CCC: $27.50
Published on Web 06/10/2004

higher than that of Al-based systems. The higher weight percentage of hydrogen in $LiBH_4$ makes it an attractive candidate for hydrogen storage. Zuttel and co-workers recently tested the hydrogen storage properties of $LiBH_4$-based systems.[51,52] They obtained an activation energy of 156 kJ/mol from thermal desorption spectra by assuming that the kinetics of hydrogen desorption is first order. Although these authors demonstrated that 13 wt % hydrogen can be released from $LiBH_4$ catalyzed by SiO_2 at about 200 °C, reversible hydrogenation has not been achieved.

Structural information is critical in understanding materials properties and performance. To experimentally determine the structure of materials involving hydrogen is extremely challenging. To track the *chemistry* of hydrogen at the atomic scale is even more difficult. On the other hand, computational chemistry and molecular simulation are advantageous for studies of well-defined model systems, including those containing hydrogen. The first principles approaches developed on the basis of density functional theory (DFT) and implemented for both clusters and periodic slabs have been applied to a wide range of problems with practical interests.[55−56] DFT calculations have been used to elucidate complex catalytic reaction mechanisms and even suggest new material leads.[57−59] Similar approaches were also used to determine the location of light atoms in chemisorbed (deuterated) benzene on Ru(0001) by combining them with the indirect information from low-energy electron diffraction.[60]

Periodical DFT calculations will be used to follow the structural and chemical changes in $LiBH_4$. The understanding of these changes helps to provide an insight to the underlying mechanism of hydrogen storage in alanate-type materials. In the present paper, the bulk structure of $LiBH_4$ was determined based on the initial structures from the synchrotron X-ray diffraction experiments. Various low-index surfaces were created on the basis of the theoretically predicted bulk structure. Structures and relative stability of these surfaces as well as the energy cost to create hydrogen vacancies have also been studied.

2. Computational Details

The DFT electronic structure calculations have been carried out using the Vienna ab initio simulation package (VASP),[61−64] a plane-wave code with a projector-augmented wave[65,66] describing nuclei and core electrons. The periodic plane-wave code is well-suited for modeling crystalline structures. On the other hand, aperiodic systems such as surfaces and defects can be modeled by carefully building a sufficiently large "super structure" as the unit cell.[67,68]

Gradient-corrected exchange-correlation functionals such as PW91,[69] PBE,[70] and revPBE[71] are implemented in VASP. Both PW91 and PBE functionals have been used self-consistently in the present study. The differences in the energetics and structures of using the two functionals were found to be negligible, and the results reported here were computed with the PBE functional.[70] An electronic smearing of 0.1 eV was employed to improve convergence of electronic self-consistent cycles. For bulk and surface calculations, the Monkhorst−Pack scheme was used to generate k-points. A separation of less than 0.05 $Å^{-1}$ between two adjacent k-points in any directions was ensured throughout the calculations.[72] A geometry optimization was considered converged when the maximum force on the movable atoms was less than 0.05 eV/Å. A cutoff energy of 400 eV was employed in the calculations. Test calculations using a cutoff energy of 600 eV showed that the plane-wave basis is well converged at 400 eV. The calculated bond strength of H_2 is 4.538 eV, without including zero-point energy (ZPE). This bond strength became 4.267 eV if ZPE was approximated as a harmonic oscillator. These values are in good agreement with the experimental results.[73]

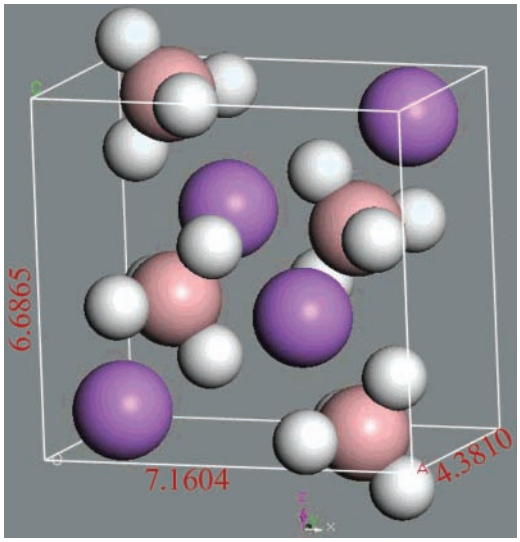

Figure 1. DFT relaxed bulk structure of orthorhombic $LiBH_4$. The dimension of the cell is labled with a unit in angstroms. The small white spheres represent H atoms, and the large purple and coral spheres represent Li and B atoms, respectively.

3. Results and Discussion

3.1. Bulk. Figure 1 shows the relaxed bulk unit cell of orthorhombic $LiBH_4$. This unit cell contains four formulas of $LiBH_4$. Two similar initial structures[45,51] were used as starting geometry to obtain the relaxed unit cell. The relaxation was considered converged when the change of the total energy is less than 10^{-4} eV. The two initial structures converged to the same structure after optimization. The unit cell of the optimized bulk structure has dimensions of $a = 7.1604$, $b = 4.3810$, and $c = 6.6865$ Å, corresponding to a volume of 209.7 $Å^3$ and a theoretical density of 0.689 g/cm^3. This optimized cell is about 3% smaller than the size determined from synchrotron powder diffraction data.[45,51] Although no symmetry was imposed during the optimization, the relaxed bulk unit cell of $LiBH_4$ has a symmetry group of *Pnma* (62) with a tolerance of 0.02 Å. In general, the calculated results are in good agreement with both sets of results obtained from the synchrotron powder diffraction. There are differences between these results and those of diffraction, in particular with regard to the positions of hydrogen atoms. The calculated B−H bonds in BH_4^- are shorter (three at 1.224 Å and one at 1.230 Å) than the corresponding bond length from the experimental data.[51] Table 1 compares the unit cell dimensions and the relative positions of the atoms in the unit cell from the present calculation with those from the previous studies.[45−51]

Charge density analysis of bulk $LiBH_4$ showed that this system has a strong ionic character. Lithium is positively charged (0.68 electron/atom) while boron is negatively charged (0.51 electron/atom). Hydrogen atoms are also negatively charged, but the amount of charge is small, ∼0.04 electron/atom. A detailed analysis of the density of states (DOS), shown in Figure 2, indicates that the covalent interaction between the 2s orbitals of the boron atom and the 1s electrons of the hydrogen atom dominates the states at the bottom of the valence band interactions. As the energy moves up, the interaction between 2p orbitals of the boron atom and the 1s electrons of

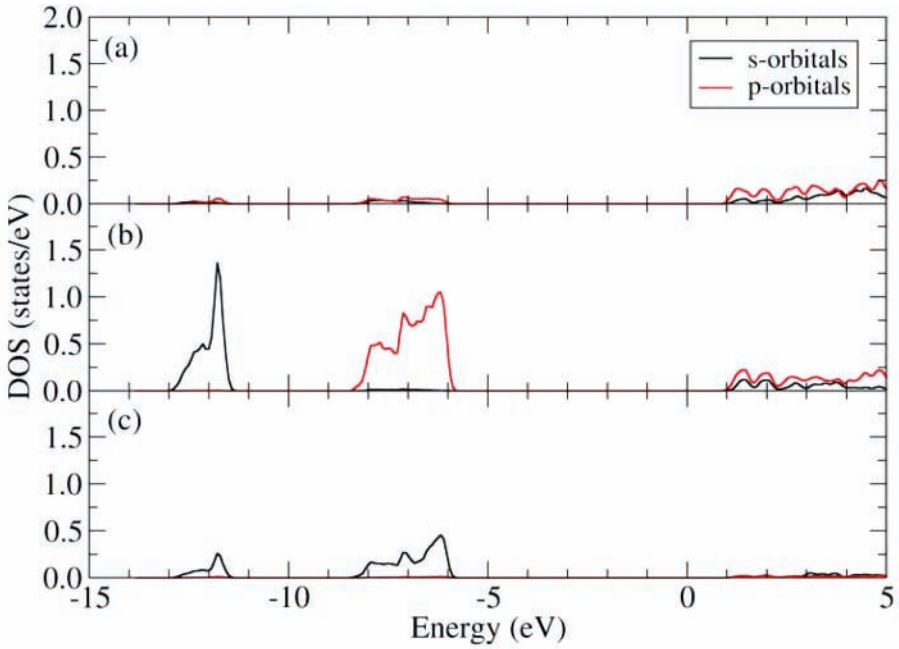

Figure 2. s- and p-projected local DOS of bulk LiBH4 at different atomic sites. (a) Li, (b) B, and (c) H.

TABLE 1: Structure Parameters of Orthorhombic LiBH4 (Results from Synchrotron Powder Diffraction Data Are Also Listed for Comparison)

	x/*a*			*y*/*b*			*z*/*c*		
	present study	ref 45	ref 51	present study	ref 45	ref 51	present study	ref 45	ref 51
	$a = 7.1604$ Å	$a = 7.17858$ Å	$a = 7.1730$ Å	$b = 4.3810$ Å	$b = 4.43686$ Å	$b = 4.4340$ Å	$c = 6.6865$ Å	$c = 6.80321$ Å	$c = 6.7976$ Å
Li	0.1568	0.1568	0.146	0.25	0.25	0.25	0.1128	0.1015	0.099
B	0.3080	0.3040	0.306	0.25	0.25	0.25	0.4270	0.4305	0.415
H1	0.9104	0.900	0.934	0.25	0.25	0.25	0.9263	0.956	0.954
H2	0.4012	0.404	0.424	0.25	0.25	0.25	0.2725	0.280	0.243
H3	0.2066	0.172	0.153	0.02497	0.054	0.104	0.4273	0.428	0.453

the hydrogen atom starts to take over. The mixing of Li s orbitals with s orbitails of H and s and p orbitals of B spans the entire energy range. The wide band gap of ~6.5 eV clearly correlates with its insulating nature.

$LiBH_4$ releases hydrogen by undergoing the following reactions

$$LiBH_4(s) \rightarrow LiH(s) + B(s) + {}^3/_2H_2(g) \qquad (13.8\ wt\%) \quad (R4)$$

or

$$LiBH_4(s) \rightarrow Li(s) + B(s) + 2H_2(g) \qquad (21.5\ wt\%) \quad (R5)$$

To obtain the heat or enthalpy of the reactions, the bulk and molecular properties of intermediates and products, including Li(s), LiH(s), B(s), and H_2(g), are also calculated. On the basis of the calculated total energies of the products, both reactions (R4 and R5) were found to be endothermic, with reaction energies of 115.4 and 195.1 kJ/mol, respectively. The measured enthalpy of formation for $LiBH_4$ at standard conditions (298.15 K, 1 atm) corresponding to that of the backward reaction of R5 is −190.8 kJ/mol.[73] The heat of reaction for reaction (R4) was calculated as 100.3 kJ/mol based on the formation enthalpy of LiH(s) reported in the same table.[73] The high heats of these endothermic reactions clearly indicate that pure $LiBH_4$ cannot be used as practical hydrogen storage materials. On the other hand, the addition of dopants, similar to adding $TiCl_3$ to $NaAlH_4$, may change completely the thermodynamics of the reaction system and therefore make the $LiBH_4$-based materials potentially useful for hydrogen storage.

3.2. Ideal Surfaces. Four low-index surfaces, (001), (010), (100), and (101), have been simulated by the corresponding slabs formed from the relaxed bulk $LiBH_4$ structures. All the surfaces have been built without breaking the B−H bond of the BH_4^- unit. The thickness of the slab in each case is about 12 Å, and the vacuum region separating the slab from its periodic images is larger than 15 Å. Figure 3 shows the side views of the four surfaces after relaxation. The surface energy, in J/m^2, is calculated by the following formula

$$\sigma_{surf} = \frac{1}{2A}(E_{stoi} - nE_{bulk}) \qquad (1)$$

where A is the area of the surface unit cell, E_{stoi} is the total energy of a stoichiometric slab, and E_{bulk} is the total energy of one formnula $LiBH_4$ in the bulk. The number of $LiBH_4$ formula in the slab is represented by *n*.

The slab that was used to simulate the (001) surface has eight Li (B) layers. The unit cell of this surface has lateral dimensions of 7.1604×4.3810 Å^2. During structure optimization, the Li and B atoms in the middle two layers were fixed at their bulk positions while the Li and B atoms in the outer layers and all the H atoms were free to relax. Relaxations in the surface layers showed some oscillatory nature: the outmost Li layer relaxed inward by 0.312 Å and second layer outward by 0.125 Å. The B atomic layers exhibit a similar trend but at a smaller extent, corresponding to 0.119 and 0.082 Å for the top and second B layers, respectively. Consequently, the slab is contracted due to these relaxations, by 0.242 Å as measured by the *z* distance between the two outmost B atoms on the opposite surfaces of

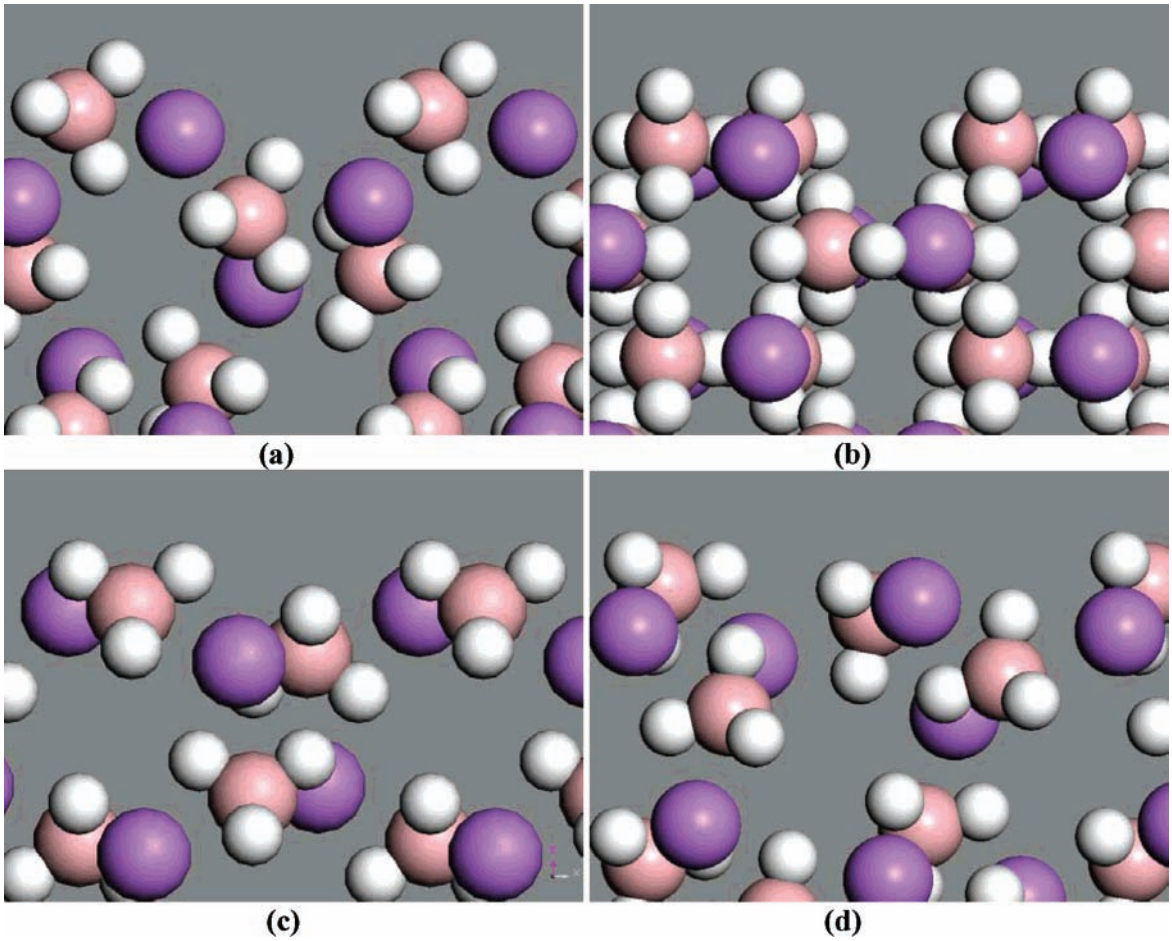

Figure 3. Side view of the (a) (001), (b) (010), (c) (100), and (d) (101) surfaces of $LiBH_4$. The small white spheres represent H atoms, and the large purple and coral spheres reresent Li and B atoms, respectively.

the slab or by 0.446 Å as measured by the *z* distance of the two outermost H atoms. In addition, the Li and B atoms in the top layers show strong lateral displacements along the ⟨100⟩ direction by 0.236 and 0.102 Å, respectively. In response to the reconstruction of Li and B atoms in the outer layers, the H atoms in these layers also restructure themselves and the extent of the displacements of H atoms is in the same order of magnitude as that of B atoms. The calculated surface energy for the (001) surface is 0.347 J/m^2.

The (010) surface was simulated by a six-layer Li (B) slab. The primitive surface unit cell size is 7.160 × 6.6865 Å^2. Similar to the (001) case discussed above, the Li and B atoms in the middle two layers of the slab were held fixed. The remaining Li and B atoms as well as all the H atoms were allowed to relax. The results showed that the top Li atomic layer relaxed inward significantly by 0.268 Å. In contrast, the top B atomic layer relaxed outward by 0.033 Å. The outward relaxation of surface B atoms resulted in a slight expansion of the slab. The lateral reconstruction of Li on (010) is strong in both directions, by 0.149 and 0.224 Å along ⟨100⟩ and ⟨001⟩, respectively. The displacements of hydrogen atoms are relatively small due to the small displacements of B atoms. The calculated surface energy of (010) is 0.119 J/m^2.

The (100) surface was also simulated with an eight-layer Li (B) slab. The surface unit cell has lateral dimensions of 6.6865 × 4.3810 Å^2. The Li and B atoms in the middle two layers were fixed at their bulk positions, while the Li and B atoms in the outer layers and all the H atoms were allowed to relax. The relaxation of the Li layers showed some oscillatory nature, the outmost Li layer relaxed inward by 0.240 Å and the second layer outward by 0.109 Å. On the other hand, the B atoms showed a different trend. All the B atoms relaxed outward slightly, with the largest displacement of 0.045 Å in the direction perpendicular to the surface. As a result of the relaxation, the B and Li atoms switched order along the surface normal. The center of the top Li atoms was higher than that of the top B atoms at the unrelaxed surface along the surface normal. The relaxation made the center of the top Li atoms lower than that of the top B atoms, as shown in Figure 3c. As the surface is more compact than the (001) surface, the lateral displacements of Li and B atoms in the top layers are all less than 0.05 Å; accordingly, the displacements of hydrogen atoms in this direction are small, similar to those of the B atoms. The calculated surface energy is 0.116 J/m^2.

The (101) surface was simulated with a 12-layer Li (B) slab. The Li and B atoms in the middle four layers were held fixed at their bulk positions, while the Li and B atoms in the outer layers and all the H atoms were allowed to relax. This surface has lateral dimensions of 4.3810 × 9.7970 Å^2. The relaxation of the Li and B layers showed some oscillatory nature but with different trends. The outmost layer Li atoms relaxed inward by 0.358 Å and the second layer outward by 0.116 Å. On the other hand, the outmost B atoms relaxed outward slightly, with a displacement of 0.017 Å, and the second layer B atoms relaxed inward by 0.094 Å. This relaxation also resulted in the Li atoms in the outer layer sinking down into the slab while the top B atoms floating at surface, as shown in Figure 3d. There is little lateral displacements along the ⟨010⟩ direction. The displacements of Li atoms along $\langle 10\bar{1}\rangle$ are, however, large, with values

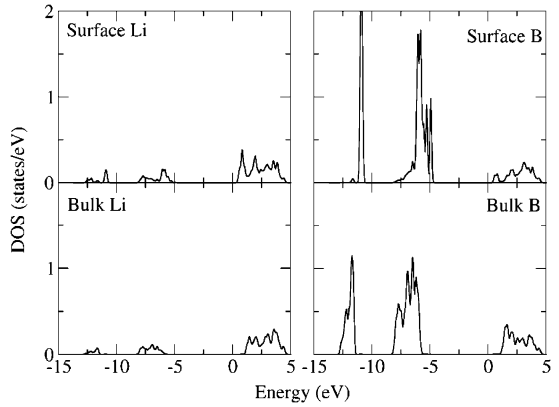

Figure 4. Comparison of local DOS of surface and bulk Li and B atoms on the (001) surface of $LiBH_4$.

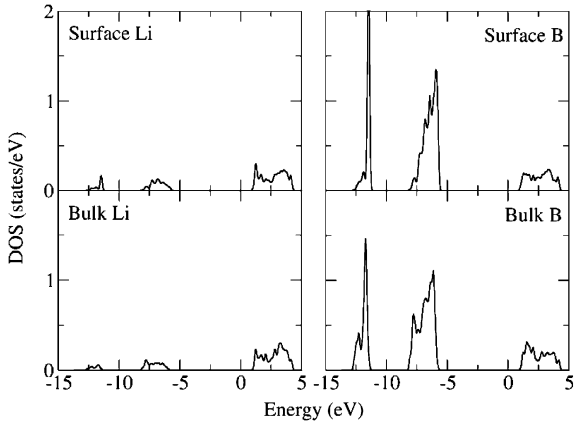

Figure 5. Comparison of the local DOS of surface and Li and B atoms in the slab simulating the (010) surface of $LiBH_4$.

of 0.133, 0.089, and 0.144 Å in the top, second, and third layers, respectively. The calculated surface energy of this surface is 0.125 J/m^2.

The charge density analysis revealed that the slabs of all four surfaces have a similar charge distribution. The Li atom close to the surface is less *positively* charged than the bulk Li atoms, while the surface B atom is less *negatively* charged. This charge redistribution upon creation of the surfaces is localized to the two surface layers, justifying the selection of slab thickness. We also compared the local DOS of the Li and B atoms that are close to the surface and those in the bulk. As shown in Figures 4 and 5, both s and p bands of the surface B atom become narrow. For the (001) surface, there is a significant shift to higher energies for both s and p bands of the surface B atom, as shown in Figure 4. Consequently, the band gap of the surface atoms is narrower than the bulk atoms. On the other hand, the local DOS of the surface B atoms in the other three surfaces exhibits a behavior that is different from the (001) surface. On these surfaces, the local DOS of the surface B atom is very similar to that of the bulk B atoms. This similarity between the surface and bulk B atoms is self-evident as shown in the Figure 5 for the (010) surface. Only the width of the bands became slightly narrow.

3.3. Hydrogen Vacancy Formation. In order for $LiBH_4$ to release hydrogen, the B−H bonds in the compound have to be broken. Therefore, the properties of the defected surfaces formed by removing H atoms from the surfaces have been studied. In general, the formation energy of H vacancies is defined as

$$\Delta E_{\mathrm{vac}} = \frac{1}{2n}\left(E_{\mathrm{vac}} - \mathrm{E}_{\mathrm{stoi}} + nE_{\mathrm{H_2}}\right) \qquad (2)$$

where E_{vac} is the total energy of the slab with hydrogen vacancy and E_{stoi} the total energy of the corresponding stoichiomrctric slab. The formation energy is averaged over the vacancies in the same unit cell, and the factor of 2 accounts for the two-sided slab. $E_{\mathrm{H_2}}$ is the total energy of a free H_2 molecule calculated in a large box.

Figure 6 gave a schematic view of forming different types of H vacancies on the (101) surface. The surface H atoms bound to the top B atom in position 1 or 2 on the original stoichiometric surface were removed, and the remaining atoms in the slab were relaxed similarly to the stoichiometric slabs. This type of vacancy was designated as Top B. The H vacancy formed by removing H atoms bound to the second-layer boron atoms (position 3) was assigned as Sub B. In addition, two vacancies were formed by removing H atoms from the positions 1 and 2 or 1 and 3. Spin-polarization has to be included for the slabs with H vacancies. The calculated formation energies of H vacancies on all four surfaces were summarized in Table 2. The H vacancy formation energies are scattered between 180 and 200 kJ/mol except for the top B hydrogen vacancy on the (001) surface. Among all the low-energy surfaces, (010) has the lowest H vacancy formation energy. The slight advantage of the (010) surface to create a H vacancy can be attributed to the larger separations between the vacancies on this surface. Although the (010) surface is not much bigger than the (101) surface in area, it has a relatively even length in both directions. The common feature of all the other three surfaces is that they share a short vector, 4.381 Å. The more evenly distributed H vacancies across the surface reduced the repulsive interaction between the vacancy and its periodic images and thereby lowered the vacancy formation energy on (010). In the remainder of the section, a detailed description for the (001) and (010) surfaces will be presented.

The formnation energy of the first H vacancy on the (001) surface is the lowest among all the cases studied. There are strong relaxations in the surface layers accompanying the creation of this H vacancy, particularly the three remaining H atoms bound to the B atom that losses its hydrogen. The structural change of these H atoms is dramatic, as shown in Figure 7b. After removing the H atom labeled 1 in Figure 7a, the remaining H atoms rotate/translate with respect to the B atoms. The H atom initially under the B atom rotated sidewise. Three H atoms and the B atom become almost coplanar after the relaxation. The structure shown in Figure 7c was formed by removing both H atoms labeled 1 and 2 in Figure 7a with subsequent relaxation. The remaining two H atoms bound to the B atom did not relax as much as in the creation of the first H vacancy. The averaged energy cost for each H atomic vacancy is 195.1 kJ/mol. In addition, our results showed that producing two H vacancies in the same unit cell by removing H atoms from both surface and subsurface B atoms has an averaged energy cost of 192.7 kJ/mol. This energy is not much more preferable than from the same B site.

To understand the origin of the structural changes, the charge density distribution as well as the local DOS was examined. It is not surprising that the most significant change occurs to the B atom that loses its hydrogen. Upon losing the H atom, the unpaired electrons were found to be localized at the B site. There is no magnetization at other atomic sites in the slab. As shown in Figure 8, there are energy splits in both s- and p-derived states of the vacant B atom. These splits produced the states that fall in the range of HOMO and LUMO energies of the bulk B atom. The appearance of these new states is at the expense of the major p-derived states that are centered at −7

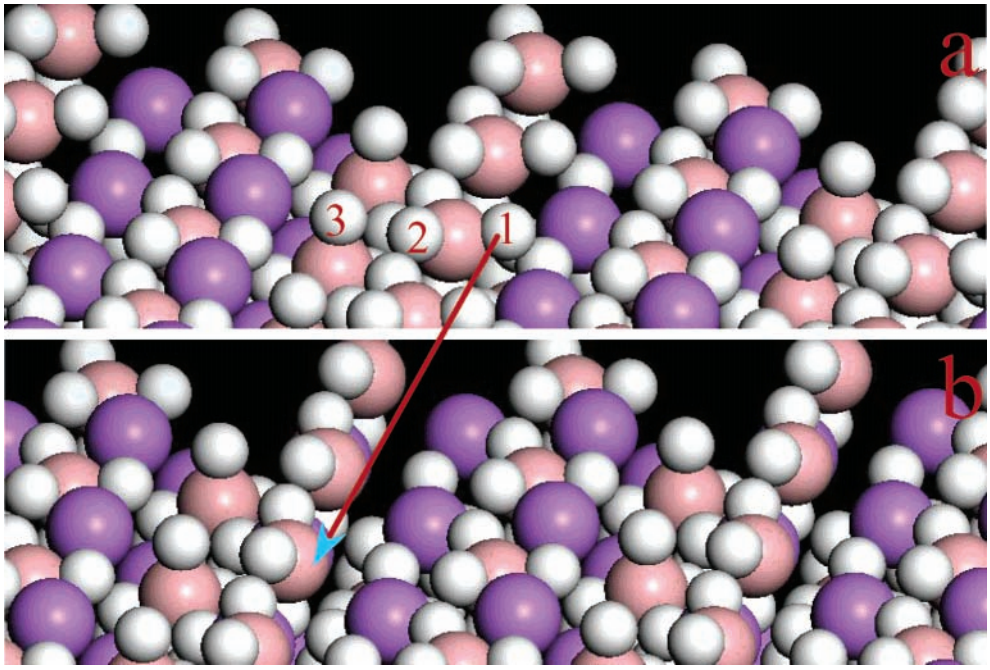

Figure 6. Schematics of H vacancy creation on the (101) surface. A row of H atoms (labled 1) were removed from the relaxed stoichiometric surface (a) to create the surface with H vacancies (b). Small white spheres represent H atoms while large purple and coral represent Li and B atoms, respectively. The surface was relaxed after the creation of the vacancies.

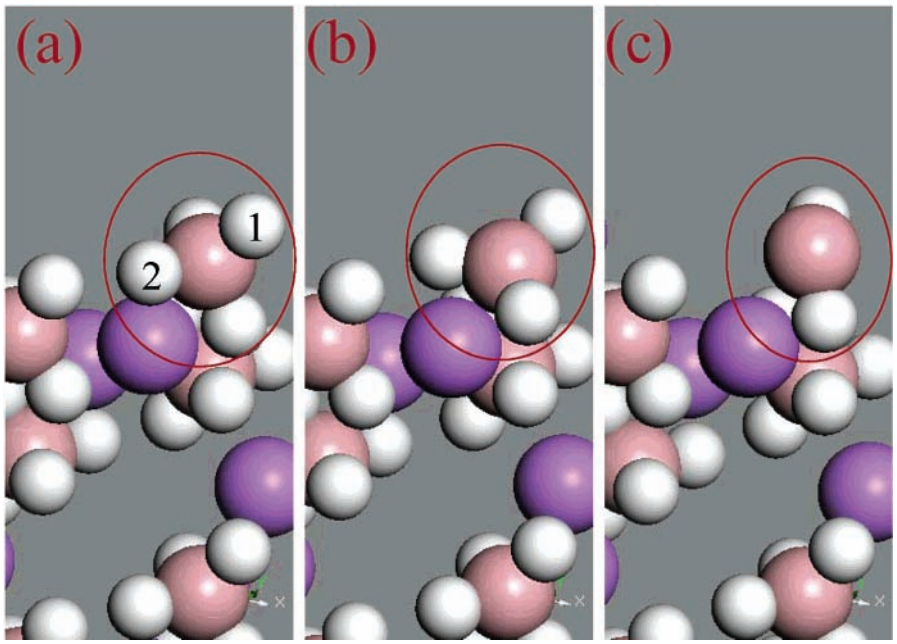

Figure 7. H vacancy formation on the (001) surface of $LiBH_4$. (a) Relaxed ideal surface, a surface BH_4^- unit is circled; (b) relaxed structure after removing H atom labled 1 from the BH_4^- unit in part a; (c) relaxed structure after removing H atoms labled 1 and 2 from the BH_4^- unit in part a.

TABLE 2: Surface Unit Cell Size, Surface Energy, and H Vacancy Formation Energy on Different Crystallographic Surfaces of LiBH4

		(001)	(010)	(100)	(101)
unit cell (Å)		7.1604 × 4.3810	7.160 × 6.6865	6.6865 × 4.3810	4.3810 × 9.7970
$\sigma_{surf}(J/m^2)$		0.347	0.119	0.116	0.125
one H vacancy	top B	165.8	182.5	192.8	187.1
	sub B			187.0	183.3
two H vacancies	same B	195.1	196.6	198.7	194.7
	different B	192.7	181.6	191.1	185.2

eV. The upper energy edge of the minority spin component of these new states is just below the Fermi level. The intensity of the s-derived band does not change much upon further oxidation of the B atom. Compared with the local DOS of one H vacancy, there is a further reduction in the intensity of the major p-derived states, as shown in the upper panel of Figure 8b. The states located in the HOMO−LUMO gap are enhanced greatly. The minority spin component is now only partially occupied. This

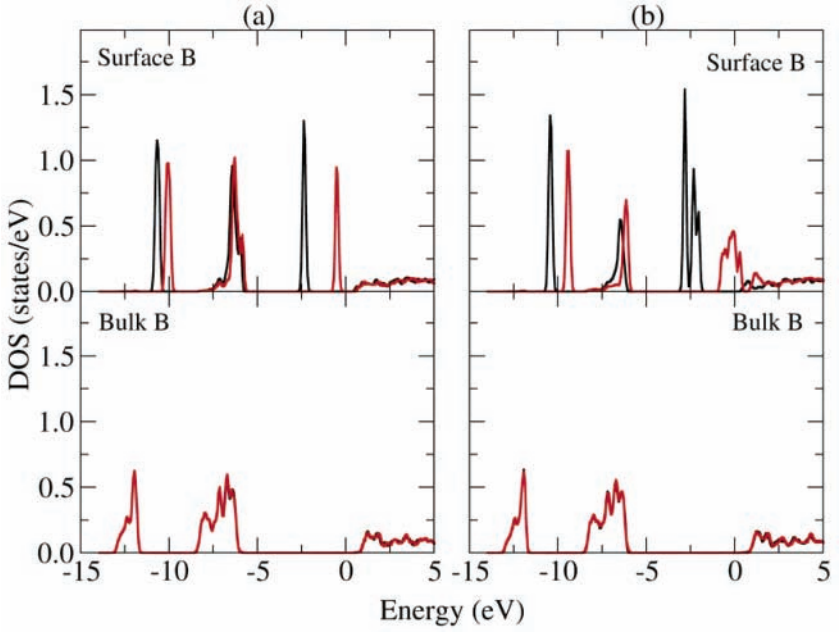

Figure 8. Spin-resolved local DOS of surface and bulk B atoms with (a) one and (b) two H vacancies on the (001) surface of $LiBH_4$. Lines in black and red correspond to the majority and minority spin component, respectively.

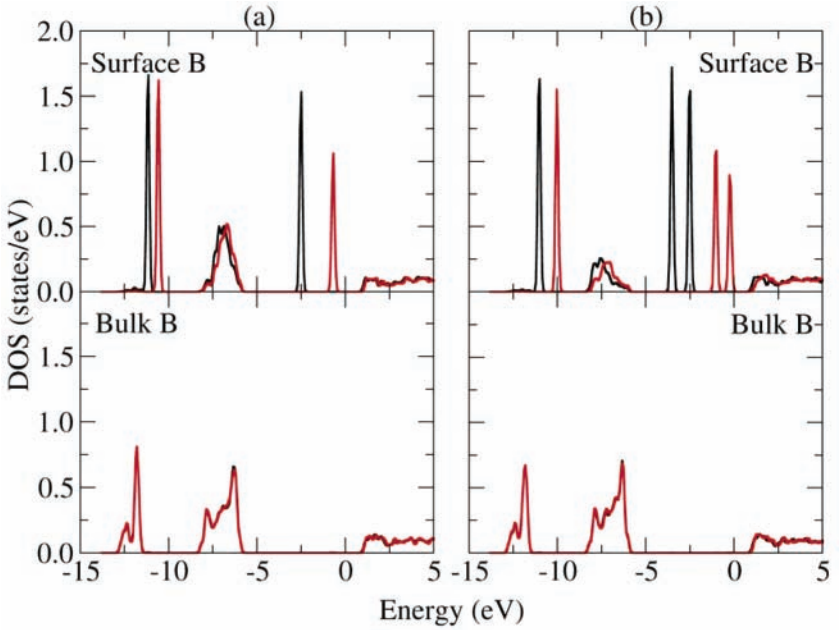

Figure 9. Spin-resolved local DOS of surface and bulk B atoms with (a) one and (b) two H vacancies on the (010) surface of $LiBH_4$. Lines in black and red correspond to the majority and minority spin components, respectively.

surface B atom has some metallic character after losing two hydrogen atoms.

The surface unit cell of the slab simulating the (010) surface contains two equivalent B atoms. The energy cost to create one H vacancy in this unit cell by removing one of the surface hydrogen atoms from one of the surface $(BH_4)^-$ units is 182.5 kJ/mol. There are also significant relaxations accompanying this change of stoichiometry. Both surface Li atoms relaxed further inward as compared with the stoichiometric surface. The most pronounced changes occurred to the hydrogen atoms bound to the B atom that loses its hydrogen atom. The remaining H atoms relaxed outward to the surface to compensate the lost hydrogen atom. They also exhibited significant lateral displacements. The energy cost for creating two H vacancies by removing two hydrogen atoms, one each from the two surface $(BH_4)^-$ units, is almost the same as that for creating one H vacancy in the same unit cell. This indicates that the $(BH_4)^-$ units in the system are relatively independent from each other and that the interactions between vacancies on this surface are weak. In contrast, the averaged energy cost for removing two hydrogen atoms bound to the same B atom is higher than that for one H vacancy or two H vacancies over two B atoms by almost 15 kJ/mol.

The charge density analysis of the surface showed that the B atom with a H vacancy is less positively charged and the unpaired electrons are localized to the B atom. The induced magnetization on the other atoms in the system is negligible. In Figure 9, a spin-resolved local DOS of the B atom with different number of H vacancies was plotted and compared with that of the B atoms in the middle of the slab, bulk B atoms. There are some similarities between Figures 8 and 9. The energy-level splits occurred in both s- and p-derived states at the vacant B site. The intensity of the s-derived states was kept

almost constant upon further oxidation of the B atom. The split of p-derived states reduced the intensity of the main peak centered at −7 eV. More new states appeared upon further oxidation in the range of the HOMO−LUMO energy gap of the bulk B atoms. The upper edge of the minority spin components remains to be below the Fermi level even when the B atom losses two hydrogen atoms.

4. Conclusion

In this paper, the properties of the bulk $LiBH_4$ and its surfaces have been studied using the periodic DFT method. The DFT-optimized bulk structure is in good agreement with the structures determined from the X-ray/synchrotron diffraction data. Four low-index surfaces were created from the predicted bulk structure. The calculated surface energy of these low-index surfaces showed that the (001) surface is the least stable. The other three surfaces, (010), (100), and (101), have similar surface energies of $\sim$0.12 J/m^2. The low surface energy of the surfaces indicates that the energy costs to create these surfaces by only breaking H−Li bonds in bulk $LiBH_4$ are not high.

The energy cost to create a single H vacancy in the low-energy surfaces, (010), (100), and (101), is scattered in a narrow range between 180 and 200 kJ/mol. This energy represents the low limit of the activation energy for hydrogen release from an ideal surface of $LiBH_4$. On the other hand, the relatively high vacancy formation energy on all these surfaces indicates that desorption of hydrogen from the crystalline surface needs to overcome high energy barriers. The activation energy of hydrogen desorption depends on the crystalline surfaces that are exposed. The particle size distribution, nonstoichiometric compositions, as well as any impurities that might exist in a real sample are expected to influence the thermodynamics and kinetics of hydrogen release/uptake. These effects will be explored in our future study.

Acknowledgment. The support from the startup funds of Southern Illinois University, Carbondale is gratefully acknowledged.

References and Notes

(1) DOE. http://www.eere.energy.gov/hydrogenandfuelcells/hydrogen/storage.html. 2003.
(2) Schlapbach, L.; Zuttel, A. *Nature* **2001**, *414*, 353.
(3) Schlapbach, L. *MRS Bull.* **2002**, *27*, 675.
(4) Yamamoto, S.; Fukai, Y.; Ronnebro, E.; Chen, J.; Sakai, T. *J. Alloys Compd.* **2003**, *356*, *697*.
(5) Saita, I.; Li, L. Q.; Saito, K.; Akiyama, T. *J. Alloys Compd.* **2003**, *356*, 490.
(6) Ratishvili, I.; Namoradze, N. *J. Alloys Compd.* **2003**, *356*, 87.
(7) Orgaz, E. *J. Alloys Compd.* **2003**, *356*, 191.
(8) Noritake, T.; Towata, S.; Aoki, M.; Seno, Y.; Hirose, Y.; Nishibori, E.; Takata, M.; Sakata, M. J. *Alloys Compd.* **2003**, *356*, 84.
(9) Majer, G.; Eberle, U.; Kimmerle, F.; Stanik, E.; Orimo, S. *Physica B* **2003**, *328*, 81.
(10) Lototsky, M. V.; Yartys, V. A.; Marinin, V. S.; Lototsky, N. M. *J. Alloys Compd.* **2003**, *356*, 27.
(11) Bowman, R. C.; Fultz, B. *MRS Bull.* **2002**, *27*, 688.
(12) Joubert, J. M.; Latroche, M.; Percheron-Guegan, A. *MRS Bull.* **2002**, *27*, 694.
(13) Akiba, E.; Okada, M. *MRS Bull.* **2002**, *27*, 699.
(14) Okada, M.; Kuriiwa, T.; Kamegawa, A.; Takamura, H. *Mater. Sci. Eng. A* **2002**, *329*, 305.
(15) Noritake, T.; Aoki, M.; Towata, S.; Seno, Y.; Hirose, Y.; Nishibori, E.; Takata, M.; Sakata, M. *Appl. Phys. Lett.* **2002**, *81*, 2008.
(16) Morinaga, M.; Yukawa, H. *Mater. Sci. Eng. A* **2002**, *329*, 268.
(17) Haussermann, U.; Blomqvist, H.; Noreus, D. *Inorg. Chem.* **2002**, *41*, 3684.
(18) Klassen, T.; Oelerich, W.; Bormann, R. Nanocrystalline Mg-based hydrides: HIydrogen storage for the zero-emission vehicle. In *Metastable, Mechanically Alloyed and Nanocrystalline Materials, Ismanam-2000*; Trans Tech Publications: 2001; Vol. 360−3, p 603.
(19) Oelerich, W.; Klassen, T.; Bormann, R. *Adv. Eng. Mater.* **2001**, *3*, 487.
(20) Oelerich, W.; Klassen, T.; Bormann, R. *Mater. Trans.* **2001**, *42*, 1588.
(21) Zeng, K. J. Klassen, T.; Oelerich, W.; Bonrmann, R. *J. Alloys Compd.* **1999**, *283*, 151.
(22) Zeng, K.; Klassen, T.; Oelerich, W.; Bormann, R. *Int. J. Hydrogen Energy* **1999**, *24*, 989.
(23) Gupta, M. *J. Alloys Compd.* **1999**, *293*−*295*, 190.
(24) Guther, V.; Otto, A. *J. Alloys Compd.* **1999**, *293*−*295*, 889.
(25) Sandrock, G. *J. Alloys Compd.* **1999**, *295*, 877.
(26) Barkhordarian, G.; Klassen, T.; Bormann, R. *Scripta Materialia* **2003**, *49*, 213.
(27) Finholt, A. E.; Bond, A. C.; Schlesinger, H. I. *J. Am. Chem. Soc.* **1947**, *69*, 1199.
(28) Bogdanovic, B.; Schwickardi, M. *J. Alloys Compd.* **1997**, *253*−*254*, 1.
(29) Bogdanovic, B.; Brand, R. A.; Marjanovic, A.; Schwickardi, M.; Tolle, J. J. *Alloys Compd.* **2000**, *302*, 36.
(30) Bogdanovic, B.; Felderhoff, M.; Germann. M.; Hartel, M.; Pomrnmerin, A.; Schuth, F.; Weidenthaler, C.; Zibrowius, B. *J. Alloys Compd.* **2003**, *350*, 246.
(31) Bogdanovic, B.; Felderhoff, M.; Kaskel, S.; Pomnmerin, A.; Schlichte, K.; Schuth, F. *Adv. Mater.* **2003**, *15*, 1012.
(32) Fichtner, M.; Fuhr, O.; Kircher, O.; Rothe, J. *Nanotechnology* **2003**, *14*, 778.
(33) Gadre, S. A.; Ebner, A. D.; Al-Muhtaseb, S. A.; Ritter, J. A. *Ind. Eng. Chem. Res.* **2003**, *42*, 1713.
(34) Genma, R.; Uchida, H. H.; Okada, N.; Nishi, Y. *J. Alloys Compd.* **2003**, *356*, 358.
(35) Gross, K. J.; Majzoub, E. H.; Spangler, S. W. *J. Alloys Compd.* **2003**, *356*, 423.
(36) Hauback, B. C.; Brinks, H. W.; Jensen, C. M.; Murphy, K.; Maeland, A. J. *J. Alloys Compd.* **2003**, *358*, 142.
(37) Lovvik, O. M. *J. Alloys Compd.* **2003**, *356*, 178.
(38) Majzoub, E. H.; Gross, K. J. *J. Alloys Compd.* **2003**, *356*, 363.
(39) Opalka, S. M.; Anton, D. L. *J. Alloys Compd.* **2003**, *356*−*357*, 486.
(40) Vajeeston, P.; Ravindran, P.; Vidya, R.; Fjellvag, H.; Kjekshus, A. *Appl. Phys. Lett.* **2003**, *82*, *2257*.
(41) Gross, K. J.; Thomas, G. J.; Jensen, C. *M. J. Alloys Compd.* **2002**, *330*−*332*, 683.
(42) Gomes, S.; Hagemann, H.; Yvon, K. *J. Alloys Compd.* **2002**, *346*, 206.
(43) Gross, K. J.; Sandrock, G.; Thomas, *G. J. J. Alloys Compd.* **2002**, *330*, 691.
(44) Hauback, B. C.; Brinks, H. W.; Fjellvag, H. *J. Alloys Compd.* **2002**, *346*, 184.
(45) Soulie, J.-P.; Renaudin, G.; Cerny, R.; Yvon, K. *J. Alloys Compd.* **2002**, *346*, 200.
(46) Sandrock, G.; Gross, K.; Thomas, G. *J. Alloys Compd.* **2002**, *339*, 299.
(47) Chen, J.; Kuriyama, N.; Xu, Q.; Takeshita, H. T.; Sakai, T. *J. Phys. Chem. B* **2001**, *105*, 11214.
(48) Bogdanovic, B.; Brand, R. A.; Marjanovic, A.; Schwickardi, M.; Tolle, J. *J. Allloys Compd.* **2000**, *302*, 36.
(49) Sun, D. L.; Kiyobayashi, T.; Takeshita, H. T.; Kuriyama, N.; Jensen, C. M. *J. Alloys Compd.* **2002**, *337*, L8.
(50) Brinks, H. W.; Hauback, B. C.; Norby, P.; Fjellvag, H. *J. Alloys Compd.* **2003**, *351*, 222.
(51) Zuttel, A.; Rentsch, S.; Fischer, P.; Wenger, P.; Sudan, P.; Mauron, P.; Emnmenegger, C. *J. Alloys Compd.* **2003**, *356*, *515*.
(52) Zuttel, A.; Wenger, P.; Rentsch, S.; Sudan, P.; Mauron, P.; Emmenegger, C. *J. Power Sources* **2003**, *118*, 1.
(53) Morioka, H.; Kakizaki, K.; Chung, S. C.; Yamada, A. *J. Alloys Compd.* **2003**, *353*, 310.
(54) Fichtner, M.; Fuhr, O.; Kircher, *O. J. Alloys Compd.* **2003**, *356*, 418.
(55) Ge, Q. F.; Kose, R.; King, D. A. Adsorption energetics and bonding from femtomole calorimetry and from first principles theory. In *Advances in Catalysis*; Knozinger, H., Ed.; Academic Press Inc: San Diego, 2000; Vol. 45, p 207.
(56) Hanmmer, B.; Norskov, J. K. Theoretical surface science and catalysis - Calculations and concepts. In *Advances in Catalysis*; Knozinger, H., Ed.; Academic Press Inc: San Diego, 2000; Vol. 45, p 71.
(57) Ceder, G.; Chiang, Y.-M.; Sadoway, D. R.; Aydinol, M. K.; Jang, Y.-I.: Huang, Q. *Nature* **1998**, *392*, 694.
(58) Besenbacher, F.; Chorkendorff, I.; Clausen, B. S.; Hammer, B.; Molenbroek, A. M.; Norskov, J. K.; Stensgaard, I. *Science* **1998**, *279*, 1913.

(59) Neurock, M. *J. Catal.* **2003**, *216*, 73.
(60) Held, G.; Braun, W.; Steinruck, H. R.; Yamagishi, S.; Jenkins, S. J.; King, D. A. *Phys. Rev. Lett.* **2001**, 8721.
(61) Kresse, G.; Hafner, J. *Phys. Rev. B* **1993**, *48*, 13115.
(62) Kresse, G.; Hafner, J. *Phys. Rev. B* **1993**, *47*, 558.
(63) Kresse, G.; Furthmuller, J. *Comput. Mater. Sci.* **1996**, *6*, 15.
(64) Kresse, G.; Joubert, D. *Phys. Rev. B* **1999**, *59*, 1758.
(65) Blochl, P. E. *Phys. Rev. B* **1994**, *50*, 17953.
(66) Hobbs, D.; Kresse, G.; Hafner, J. *Phys. Rev. B* **2000**, *62*, 11556.
(67) Payne, M. C.; Teter, M. P.; Allan, D. C.; Arias, T. A.; Joannopoulos, J. D. *Rev. Mod. Phys.* **1992**, *64*, 1045.
(68) Zhang, W. Q.; Ge, Q. F.; Wang, L. C. *J. Chem. Phys.* **2003**, *118*, 5793.
(69) Perdew, J. P.; Chevary, J. A.; Vosko, S. H.; Jackson, K. A.; Pederson, M. R.; Singh, D. J.; Fiolhais, C. *Phys. Rev. B* **1992**, *46*, 6671.
(70) Perdew, J. P.; Burke, K.; Ernzerhof, M. *Phys. Rev. Lett.* **1996**, *77*, 3865.
(71) Hammer, B.; Hansen, L. B.; Norskov, J. K. *Phys. Rev. B* **1999**, *59*, 7413.
(72) Monkhorst, H. J.; Pack, J. D. *Phys. Rev. B* **1976**, *13*, 5188.
(73) Lide, D. R. *CRC Handbook of Chemistry and Physics*; CRC Press: Boca Raton, 2004; Vol. 84.